Journal of Materials Chemistry C

ROYAL SOCIETY OF CHEMISTRY

PAPER

View Article Online
View Journal | View Issue

Cite this: *J. Mater. Chem. C*, 2023, **11**, 5438

Electro-optic properties of polystyrene particle-laden polymer-stabilized liquid crystals†

Alexandra Gruzdenko and Ingo Dierking *

Received 7th February 2023,
Accepted 1st April 2023

DOI: 10.1039/d3tc00437f

rsc.li/materials-c

Particle-laden polymer-stabilized liquid crystal (PLPSLC) composites were studied as a means to improve the electro-optic properties of nematic liquid crystals. Polystyrene nanaparticles possesing no distinctive physical properties were chosen as nanodopants in order to investigate effects caused solely by the physical presence of nanoobjects. The threshold voltage, response times, relevant physical properties, and optical textures were characterized first for polymer-stabilized and particle-laden liquid crystals (PSLCs and PLLCs) made of target materials and then for PLPSLCs. Polymer stabilization allowed one to dramatically decrease the overall response time but at the cost of the increased threshold voltage. The particles alone appeared not to change the properties significantly. At the same time, when the particles and polymer were used together, interesting effects were observed: the threshold voltage could be reduced by up to two times in comparison to a polymer-stabilized liquid crystal (PSLC) while the advantage of the fast overall response time intrinsic to PSLCs was retained. A possible explanation for such behaviour can be a decrease in the effective polymer concentration caused by either the particle-induced distortion or particle-induced sparsening of the polymer network. Overall, the reported results help to shed light on how simple nanoparticles interact with the polymer network and liquid crystal. This knowledge can potentially aid the creation of more complex PLPSLC composites with desired properties in the future.

1. Introduction

Liquid crystals (LCs) are well-known for their applications in optic technologies which include displays,[1] smart windows,[2] terahertz filters,[3] photonic crystals,[4] optical gratings,[5] lasers,[6] and others. With the aim of improving the characteristics of these devices and developing new technological concepts, various composites of liquid crystals and other materials are being studied. In particular, the possibility to optimize the electro-optic properties of nematic liquid crystals, which are widely used in LC applications, by adding additional components to them is often investigated. Polymers and colloids, which, as well as LCs, belong to the class of soft matter materials, are usually used as the additives.

Polymer–liquid crystal composites are commonly divided into polymer-dispersed and polymer-stabilized liquid crystals (PDLCs and PSLCs).[7] Polymer rich PDLCs consist of a polymer matrix with liquid crystal droplets dispersed within it while LC rich PSLCs comprise a polymer network filled with a liquid crystal. Since, in contrast to PDLCs, the alignment of liquid crystal molecules is not disturbed in PSLCs, the latter are considered to be more suitable for tuning the electro-optic properties.

The influence of polymer stabilization on the electro-optic performance has been investigated for different devices based on nematic liquid crystals including the homogeneous,[8,9] vertically aligned,[10] in-plane switching,[11] and twisted nematic cells.[12] For many of the devices, the polymer network has allowed one to significantly decrease at least one of the response times and eliminate some undesirable effects such as the back-flow. However, the introduction of a polymer has also led to higher driving voltages, a decreased device transmittance, and often increased scattering. Therefore, the composition of PSLCs usually needs to be optimized to reach the balance between the advantages and disadvantages.

The combination of LCs and colloids, which will be termed particle-laden liquid crystal (PLLC) in this work, comprises nanoparticles dispersed in a liquid crystal. A wide range of nanodopants has been used in studies on PLLCs including ferroelectric,[13] metal,[14] metal oxide[15] nanoparticles, quantum dots,[16] and carbon nanomaterials such as fullerenes,[17] carbon nanotubes,[18] and graphene oxide flakes.[19] For all cases, an improvement not only in the electro-optic but also in physical properties has been reported in many articles. For example, it has been shown that the threshold voltage and response times

The University of Manchester, Oxford Rd, Manchester, M13 9PL, UK.
E-mail: ingo.dierking@manchester.ac.uk

† Electronic supplementary information (ESI) available. See DOI: https://doi.org/10.1039/d3tc00437f

can be lowered; the dielectric anisotropy can be increased enhancing the effective anisotropy of the system; the nematic–isotropic phase transition temperature often becomes higher increasing the stability of the nematic phase.[13–15,17–19] However, the adverse and null effects on the properties have also been reported.[20–22] Notably, different behaviour can be observed for the same type of nanoparticles and even for the same pairing of particles and liquid crystal.[23,24] The inconsistency in the results is usually caused by the high sensitivity of PLLC systems to the experimental and material parameters.

Overall, both polymer-stabilized and particle-laden liquid crystals have been extensively investigated in terms of electro-optic properties, and the advantages and limitations of these types of composites are generally understood. Therefore, a natural step forward is to combine all the three soft matter materials together, and particle-laden polymer-stabilized liquid crystals (PLPSLCs) indeed start to emerge as a research direction. The few existing studies[25–33] have demonstrated that PLPSLCs can not only decrease the threshold voltage and response times compared to PSLC systems[25–27] but also suppress particle-induced hysteresis effects and the formation of large particle aggregates thus increasing the device transmittance.[28] Moreover, a temperature independent threshold voltage has been reported for PLPSLCs in which nanoparticles have been incorporated into polymer strands.[30,31] However, further research is still necessary to reveal the full potential of these materials and understand their behaviour in detail.

To establish reliable methods of producing PLPSLC composites with desired properties, one needs to understand how nanoparticles, the polymer network, and liquid crystal influence each other. Therefore, we decided to study the case of relatively simple PLPSLC composites doped with polystyrene nanoparticles which do not possess any specific physical properties. This should allow one to characterise the pure effect of the physical presence of nanoobjects in a PLPSLC system. The dependence of the threshold voltage and response times on the particle concentration at a fixed polymer content was investigated. Optical textures and some relevant physical properties including the splay elastic constant, rotational viscosity, dielectric constants, and nematic–isotropic transition temperature were also characterised to aid the interpretation of the results. For consistency, the properties of PSLC and PLLC composites made of the target materials were first studied.

2. Experimental

2.1 Materials

Nematic liquid crystal 5CB (4-Cyano-4'-pentylbiphenyl) with a phase sequence Cr – 22.5 °C – N – 35 °C – I was purchased from Fluorochem Ltd and used as the main component for the composites. Bifunctional, UV-curable monomer RM257 (2-methyl-1,4-phenylene bis (4-(3-(acryloyloxy) propoxy) benzoate)) with a phase sequence Cr – 70 °C – N – 126 °C – I and photoinitiator benzoin methyl ether were used as materials for polymer networks and procured from Synthon Chemical and Sigma Aldrich, respectively. Polystyrene (PS) nanospheres of 150 nm in diameter were purchased from Polysciences in the form of a water-based dispersion stabilized by an ionisable surfactant containing sulfate ester. The surfactant molecules covered the particles and gave them a slight anionic charge due to the surfactant dissociation into ions.

5 μm thick homogeneous cells made of two glass slides covered with ITO and antiparallelly rubbed polyimide layers were purchased from AWAT (Poland) and used to prepare samples.

2.2 Sample preparation

2.2.1 Liquid crystal sample. 5CB was filled in a cell by the capillary method. During the filling process, the liquid crystal was kept at 60 °C to ensure that the material was in the isotropic state. Afterwards, the sample was cooled to the nematic phase.

2.2.2 Particle-laden liquid crystal samples. To prepare PLLC composites, the particles were transferred to the liquid crystal by means of a solvent. Isopropanol was chosen for this purpose since it does not destroy polystyrene. First, a small amount of the initial particle–water dispersion was diluted with a much larger amount of isopropanol to prepare a 0.1 mg mL^{-1} particle-isopropanol dispersion. The mixture was sonicated in an ultrasonic bath (Sonomatic) for 1 h, and then the size distribution of particles in the system was characterized by the method of dynamic light scattering (DLS) (Zetasizer Nano system). The average particle size (*Z*-average) was found to be 165.6 ± 34.70 nm confirming the acceptable quality of the dispersion. Then the dispersion was transferred to the liquid crystal in the isotropic phase (at 60 °C) since particle aggregation did not occur in this case. After that, the obtained mixture was always kept in this phase to avoid the aggregation. The mixture was left on a magnetic stirrer (Gallenkamp) at 60–70 °C for at least 20 h to evaporate the solvent (polystyrene glass transition and melting points are 100 °C and 270 °C, respectively, therefore, the particles would not be damaged by the heating). Then the mixture was sonicated for 2 min and stirred with a spatula for 5 min at 60 °C. At the same temperature, the composite material was filled in a cell. Only then the sample was cooled to the nematic phase. This allowed one to supress the formation of large aggregates which otherwise form naturally during the isotropic–nematic transition. It must be noted that aggregation still occurred to a certain degree. Overall, four PLLC samples with particle concentration C_{NP} of 0.01, 0.05, 0.1, and 0.2 wt% were prepared following the described method (Table 1).

2.2.3 Polymer-stabilized and particle-laden polymer-stabilized liquid crystal samples. First, a polymer–liquid crystal blend was prepared. The monomers were added directly to the liquid crystal in the proportion of 5 : 95 by weight. The mixture was sonicated for 30 min. Then the photoinitiator dissolved in isopropanol and presonicated for 1 h was added to the monomer-liquid crystal blend in the amount of 2 wt% of the monomer content. The resulting mixture was sonicated for

Table 1 Composite types and corresponding mixtures studied in the paper. PS stands for polystyrene nanoparticles

Composite type	Studied mixtures
Liquid crystal	5CB
PLLC	5CB + X wt% PS, where X = 0.01, 0.05, 0.1, 0.2
PSLC	5CB + 5 wt% RM257
PLPSLC	5CB + 5 wt% RM257 + X wt% PS, where X = 0.01, 0.05, 0.1, 0.2

30 min and then kept at 60 °C on a hot plate (IKA C-MAG HP 10) until the isopropanol had evaporated. After that the mixture was sonicated for 15 min, stirred with a magnet at 60–70 °C for 15 min, and finally mixed with a spatula for 2 min. Since the properties of a polymer network strongly depend on the polymer concentration C_p, the same mixture was used to prepare PSLC and all PLPSLC samples to minimize the discrepancy in this parameter.

A particle dispersion prepared as described in the previous section was added to parts of the polymer–liquid crystal mixture in the isotropic phase (at 60 °C) in such proportions as to get mixtures with particle concentration C_{NP} of 0.01, 0.05, 0.1, and 0.2 wt% (Table 1). After that, the mixtures were always kept in the isotropic phase to avoid particle aggregation. The mixtures were left on the magnetic stirrer at 60–70 °C for about 22 h to evaporate the isopropanol. After that, they were sonicated for 2 min and stirred with a spatula for 5 min at 60 °C. At the same temperature, they were filled in cells. The remaining polymer mixture was again sonicated for 15 min, stirred with the magnet at 60–70 °C for 15 min, mixed with a spatula for 2 min at 60 °C, and then filled in a cell at 60 °C in order to prepare a PSLC sample (Table 1). Since the network properties are strongly influenced by the polymerisation temperature, all the cells were polymerized simultaneously at 25.7 °C in the nematic phase. The polymerisation process lasted for 1.5 h. UV light of 0.06 mW cm^{-2} intensity (NeoLab UV lamp) was employed. It must be noted that the liquid crystal and PLLC samples were treated with UV light in the same way in order to take into account any possible influence of the UV irradiation on 5CB and polystyrene particles.

2.3 Experimental measurements

An LCR meter (Agilent E4980A) set to the parallel equivalent circuit mode was used to measure the dependence of the cell capacitance on the applied voltage for the composite of interest. 1 kHz sine signals of different amplitudes were used for the measurements. The threshold voltage was determined by identifying the onset of the capacitance rise occurring upon the increase in the applied voltage. All threshold voltage values presented in this paper are root mean square voltages. The capacitance values in the absence of the electric field and in the limit of its infinitely high amplitude were used to calculate $\varepsilon_\perp$ and $\varepsilon_\parallel$, respectively, from the equation for a parallel plate capacitor:

$$C = \frac{\varepsilon\varepsilon_0 S}{d} \tag{1}$$

where C is the cell capacitance, ε is the effective dielectric constant of the composite, ε_0 is the vacuum permittivity, S is the area of that part of the cell to which the electric field is applied, d is the cell gap. C corresponding to the infinitely large electric field was found by fitting the high voltage region of a $C(1/V)$ plot with $C = A - \frac{B}{V}$ where A and B are fitting parameters and extrapolating the result to $1/V = 0$ (such fitting has been justified in ref. 34). Finally, the dielectric anisotropy could be found from the formula $\Delta\varepsilon = \varepsilon_\parallel - \varepsilon_\perp$.

To measure the response times, the cell was placed on a microscope (Leica DMLP) with polarizers crossed at 90°. A 600 nm filter (Thorlab) was placed between the cell and the analyser to perform measurements with monochromatic light. A 1 kHz sine carrier signal modulated with a 450 mHz square wave was applied to the cell by a signal generator (Agilent 33220A) and amplified if necessary. The light intensity relaxation after the application and removal of the electric field was recorded using a photodiode connected to a digital oscilloscope (Tektronix TDS 2024C). The response times were found by fitting the intensity relaxation curves with theoretical equations:

$$I(t) \sim \left[\sin\left(\frac{\Delta\varphi_{off}}{2} - \frac{(\Delta\varphi_{off} - \Delta\varphi_{on})}{2}\frac{1}{1 + \left[\frac{\theta_{on}^2}{\theta_{off}^2} - 1\right]e^{-\frac{2t}{\tau_r}}}\right)\right]^2 \tag{2}$$

for the relaxation upon the electric field application and

$$I(t) \sim \left[\sin\left(\frac{\Delta\varphi_{off}}{2} - \frac{(\Delta\varphi_{off} - \Delta\varphi_{on})}{2}e^{-\frac{2t}{\tau_d}}\right)\right]^2 \tag{3}$$

for the relaxation upon the electric field removal. $\Delta\varphi_{off}$, $\Delta\varphi_{on}$ and θ_{off}, θ_{on} are the phase shifts between the ordinary and extraordinary waves and the angles between the director and cell plane in the middle of the cell in the absence and presence of the electric field, respectively; τ_r and τ_d are the rise and decay times. The derivations of eqn (2) and (3) are given in the ESI.† The theoretical expressions for the response times are:[35,36]

$$\tau_r = \frac{\gamma_1}{\varepsilon_0\Delta\varepsilon E^2 - \frac{\pi^2}{d^2}K_{11}} \tag{4}$$

and

$$\tau_d = \frac{\gamma_1 d^2}{K_{11}\pi^2} \tag{5}$$

where γ_1 is the rotational viscosity, E is the applied electric field, and K_{11} is the splay elastic constant. Since τ_r depends on E, the

property was measured using a carrier signal with a fixed root mean square amplitude of 6 V.

The splay elastic constant K_{11} was found from the equation for the threshold voltage:[35,36]

$$V_{th} = \pi\sqrt{\frac{K_{11}}{\varepsilon_0\Delta\varepsilon}}. \quad (6)$$

The rotational viscosity γ_1 was calculated from eqn (5) for the decay time.

During all the measurements discussed earlier in this subsection, the temperature of the cell was kept at 29 °C by means of a hot stage (Mettler Toledo FP82/HT).

The nematic–isotropic transition temperature T_{NI} was identified by heating the sample with the help of the hot stage and observing corresponding textural changes in the microscope. Optical images in crossed polarizers were recorded using a digital camera (IDS uEye camera, 2048 × 1088 resolution) placed on the top of the microscope. To visualize polymer networks, if any, the sample was heated just above T_{NI} into the isotropic state.

3 Results and discussion

3.1 Polymer-stabilized liquid crystal composite

3.1.1 Electro-optic properties. The electro-optic performance of the PSLC composite is compared to that of 5CB in Table 2. According to the table, the addition of the polymer network resulted in a 6-fold increase in the threshold voltage. Such behaviour is typical for PSLCs[8,9,37–41] and can be explained by an increase in the internal surface area. Indeed, the polymer strands provide an additional surface which interacts with the liquid crystal molecules and, like the orientation layers, keeps the molecules parallel to itself. Due to this fact, a higher voltage is necessary to induce the reorientation of the molecules in the electric field.

For the same reason of the additional surface interactions, the director needs more time to respond to the electric field and less time to return to the horizontal position favoured by the network and orientation layers. Therefore, a strong increase in the rise time τ_r and a very pronounced decrease in the decay time τ_d were observed.

Importantly, despite the opposite kind of behaviour for τ_r and τ_d, the overall response time $\tau_r + \tau_d$ decreased by approximately an order of magnitude.

3.1.2 Physical properties. Physical properties measured for the PSLC composite and 5CB are presented in Table 3. The dielectric anisotropy $\Delta\varepsilon$ decreased with $\varepsilon_\perp$ increasing only slightly and $\varepsilon_\parallel$ substantially going down. Similar observations have already been reported for PSLCs with the homogeneous alignment.[37–39] The slight increase in $\varepsilon_\perp$ may be caused by the polymer network contribution to the overall value of the permittivity. The decrease in $\varepsilon_\parallel$ may be related to the fact that the polymer strands significantly hinder the field-induced rotation of the liquid crystal molecules in their vicinity and also trap some molecules inside their interior. Such molecules being strongly affected by the network stay oriented almost horizontally even in the presence of the field and therefore contribute ε close to $\varepsilon_\perp^{LC}$ to the total $\varepsilon_\parallel^{PSLC}$ value. This should result in the decrease of the latter.

The splay elastic constant K_{11} became two orders of magnitude larger upon the polymer stabilisation. Such a dramatic change is common for PSLCs[9,37] and means that the system effectively became more rigid when the polymer network was introduced. At the same time, the viscosity γ_1 stayed the same in the limits of error. The slight observed increase may be caused by the presence of a small number of relatively short polymer chains which have not been incorporated into the network. The nematic–isotropic transition temperature T_{NI} was not affected by the polymer.

The optical textures of the PSLC composite will be discussed further in the text together with the textures of the PLPSLC composites.

3.2 Particle-laden liquid crystal composites

3.2.1 Optical textures. The optical textures of the PLLC samples are shown in Fig. 1(a). One can see that aggregates were present in the samples, and their number grew with increasing particle concentration C_{NP}. Moreover, at high concentrations, the aggregates started to form patterns, and at C_{NP} = 0.2 wt%, a well-established texture (Fig. 1(a-vi)) was observed in some areas of the cell although it was less pronounced in other places (Fig. 1(a-v)).

The patterns may originate from particle aggregation occurring when a sample is cooled from the isotropic to the nematic state after the cell has been filled (see Section 2.2.2 on PLLC sample preparation methods). Indeed, during the first order isotropic–nematic transition, the two phases coexist for some period of time (Fig. 1(b)). The interface between them separates

Table 2 Electro-optic properties of the 5CB + 5 wt%RM257 PSLC composite and 5CB. All measurements were taken at T = 29 °C, f = 1 kHz. The rise time τ_r was measured using a carrier signal with a root mean square amplitude of 6 V

Sample	V_{th} (V)	τ_r (ms)	τ_d (ms)
5CB	0.630 ± 0.006	0.59 ± 0.03	33.3 ± 0.2
PSLC	3.699 ± 0.006	2.1 ± 0.4	1.5 ± 0.1

Table 3 Physical properties of the 5CB + 5 wt%RM257 PSLC composite and 5CB. All measurements, except those of T_{NI}, were taken at T = 29 °C, f = 1 kHz

Sample	T_{NI} (°C)	$\varepsilon_\perp$	$\varepsilon_\parallel$	$\Delta\varepsilon$	K_{11} (pN)	γ_1, (Pa s)
5CB	34.8 ± 0.1	7.43 ± 0.07	19.78 ± 0.08	12.3 ± 0.1	4.40 ± 0.09	0.058 ± 0.001
PSLC	34.8 ± 0.1	7.51 ± 0.04	16.40 ± 0.10	8.9 ± 0.1	109 ± 1	0.063 ± 0.005

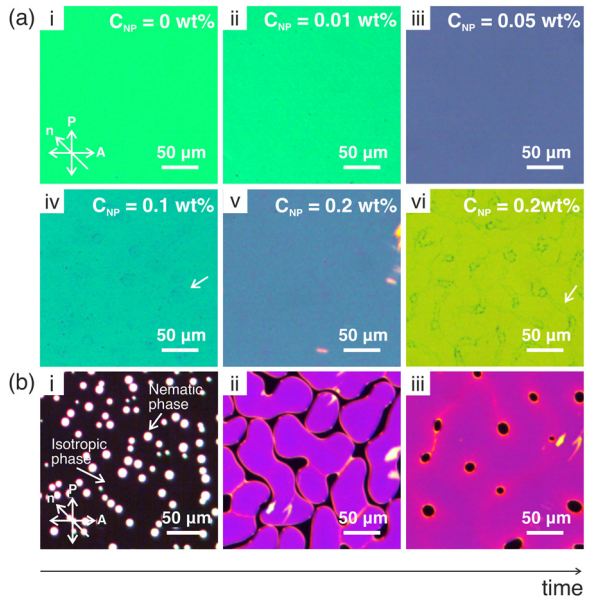

Fig. 1 (a) Polarised optical textures of the PLLC composites with different particle concentrations indicated in the images. Images (i–v) were taken at 33 °C; image (vi) was taken at 29 °C. The temperature was chosen such as to better visualize particle aggregates. White arrows point at elements of the patterns formed by the aggregates. (b) Evolution of the optical texture of the 5CB + 0.05 wt%PS PLLC composite during the transition from the isotropic to the nematic phase occurring at 34.7 °C. The transition lasted for about 10–20 seconds.

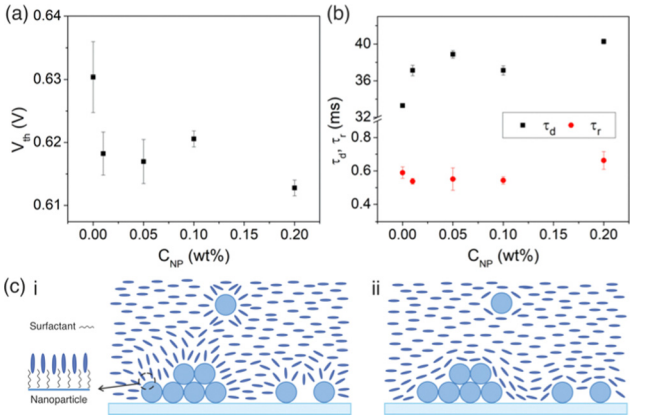

Fig. 2 Dependence of the threshold voltage V_{th} (a) and response times τ_d and τ_r (b) on the particle concentration C_{NP} for the PLLC composites. All measurements were taken at T = 29 °C, f = 1 kHz. The rise time τ_r was measured using a carrier signal with a root mean square amplitude of 6 V. (c) Distortions of the director field for the cases when the particles kept (i) and did not keep (ii) the surfactant shells. Note that while in the inset, the liquid crystal and surfactant molecules are depicted to scale, in the main figures, not liquid crystal molecules but the director is shown. The fact that the complete coverage of the glass slides by the particles is not possible at the concentrations used is taken into account in the figures.

two mediums with different physical properties and therefore may partially act as a physical wall. Such a wall should push at least some of the particles forcing them to move along with it. One can argue that if the number of particles accumulated at the interface becomes too large, reaching a certain critical value, the particles stop and in this way template the interface shape at that moment. The higher C_{NP}, the quicker this critical particle number is achieved. Therefore, only occasional, if any, dark spots corresponding to the very end of the phase transition were templated at $C_{NP} \leq 0.05$ wt%, and circle- and worm-like patterns observed at the earlier stages of the process were formed at C_{NP} = 0.1 wt% and C_{NP} = 0.2 wt%, respectively (compare Fig. 1(a-iv) and (b-iii), Fig. 1(a-vi) and (b-ii).

One can expect that some of the particles were pushed by the moving interface but did not go straight to the boundary between the two phases. Therefore, the regions inside the contours formed by the aggregates may be rich in particles.

It must be noted that similar patterns are often observed during spinodal phase separation in multi-component systems. This process occurring in PLLC systems upon quenching from the isotropic phase has been theoretically studied in several articles,[42–45] and the formation of regions rich and poor in particles has been predicted. The spinodal transition may underlie the process which we described above.

3.2.2 Electro-optic properties. The threshold voltage dependence on the particle concentration C_{NP} is shown in Fig. 2(a). V_{th} quickly decreased when even a small concentration of particles was added and then showed a slight decline upon the further increase in the particle content. At the highest particle concentration C_{NP} = 0.2 wt%, V_{th} was improved by only 3% compared to 5CB.

The threshold voltage reduction can be caused by the sedimentation of the particles and their aggregates onto the cell substrates, which is common for functionalized nanoparticles.[46–52] Once deposited onto the orientation layers, particles should modify the interactions between the liquid crystal and the substrates. Particles functionalized with mesogenic or pro-mesogenic organic molecules are known to induce the homeotropic molecular orientation due to the coupling between the organic and liquid crystal molecules (see the inset in Fig. 2(c–i)).[49–51] Hence, if in our case the particles had remained covered by the surfactant molecules (which are organic and mesogenic) after being transferred to 5CB, one could expect the distortions of the director field schematically shown in Fig. 2(c-i). On the other hand, if the particles had lost the surfactant shells but still sedimented, the planar molecular orientation would be more probable since a certain kind of surface roughness is necessary to induce the homeotropic alignment while the particles are expected to be relatively smooth. The director field corresponding to this case is shown in Fig. 2(c-ii). Further research would be necessary to distinguish between the two options. However, one can see that in both cases the angle between the molecules and the cell plane is larger than zero in the areas strongly affected by the particles. Therefore, the electric torque acting on such molecules is non-zero which should result in smaller voltages being necessary to induce the Freedericksz transition.

The behaviour of the response times is shown in Fig. 2(b). While the decay time τ_d demonstrated a rising trend and

saturated at a value which is 21% higher compared to neat 5CB, the rise time τ_r stayed practically constant. These results can be explained by the observed increase in the viscosity γ_1 (Fig. 3(c)) and concentration-independent splay elastic constant K_{11} (Fig. 3(b)), which will be discussed in more detail in the next section. Indeed, according to eqn (5), τ_d should increase with γ_1 if K_{11} stays constant. At the same time, from eqn (4) follows that τ_r should increase as well. However, the expected increasing behaviour was not observed since the experimental errors were comparable to the expected changes in τ_r which were estimated from Equation 4 using the measured values of γ_1 and K_{11}.

3.2.3 Physical properties. As can be seen in Fig. 3(a), the nanoparticles did not significantly influence the dielectric properties of the liquid crystal. This result is expected since very small particle concentrations were used. The slight increase observed for $\varepsilon_\parallel$ and $\varepsilon_\perp$ cannot be related to the particles' contribution to the overall permittivity values since $\varepsilon \approx 3$ for polystyrene[53] is smaller than $\varepsilon_\parallel^{5CB} = 19.43$ and $\varepsilon_\perp^{5CB} = 7.43$ for 5CB. However, the effect can be assigned to the particle-induced director field distortions. Indeed, the liquid crystal molecules in the vicinity of the sedimented particles are tilted relative to the cell plane and hence should contribute $\varepsilon > \varepsilon_\perp^{5CB}$ to the overall value of $\varepsilon_\perp$ increasing the latter. In the case of $\varepsilon_\parallel$, the particles may enhance the vertical alignment of the molecules increasing the permittivity if one assumes that the surfactant shells were kept. The changes in $\varepsilon_\parallel$ and $\varepsilon_\perp$ resulted in the dielectric anisotropy $\Delta\varepsilon$ also slightly increasing.

Since neither the threshold voltage nor the dielectric anisotropy showed a significant change upon the addition of the particles, the splay elastic constant K_{11} calculated from these properties also stayed practically constant (Fig. 3(b)).

The viscosity γ_1 showed a generally rising trend and at C_{NP} = 0.2 wt%, reached a value which is 16% higher than that for 5CB. The rising behaviour of the viscosity has often been observed for PLLCs.[54–57] It can result from molecular interactions between nanodopants in the bulk and liquid crystal molecules if one assumes that at least some of the nanospheres stayed dispersed despite the aggregation and sedimentation. Notably, the director distortions around the dispersed particles (see Fig. 2(c)) could also contribute to the threshold voltage reduction and changes in the dielectric constants.

The presence of the particles also caused a linear decrease in the nematic–isotropic transition temperature T_{NI} (Fig. 3(d)). The destabilizing influence of nanoobjects on the nematic phase has often been reported for particles with no or very weak anisotropic properties.[58–60] The effect can be attributed to the fact that the particles in the bulk occupy some volume, and therefore, decrease the effective number density of liquid crystal molecules, *i.e.* dilute the liquid crystal. This should lead to the reduction of the nematic order, which, in turn, should cause the decrease in the transition temperature T_{NI}.[61]

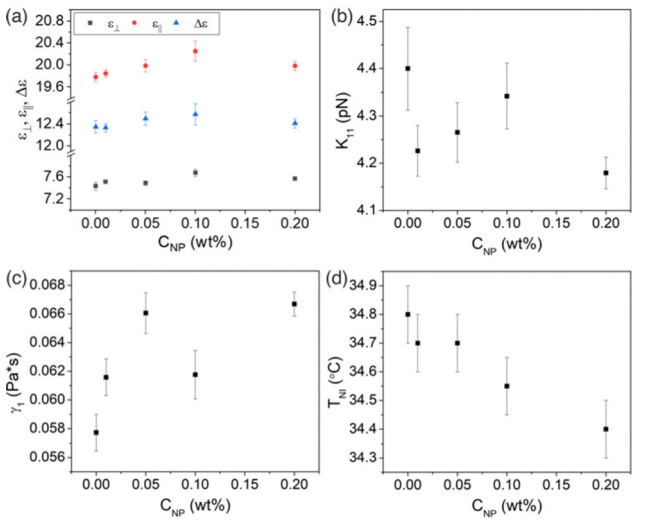

Fig. 3 Dependence of the physical properties on the particle concentration C_{NP} for the PLLC composites: (a) the dielectric constants $\varepsilon_\parallel$ and $\varepsilon_\perp$ and dielectric anisotropy $\Delta\varepsilon$, (b) the splay elastic constant K_{11}, (c) the viscosity γ_1, (d) the nematic–isotropic transition temperature T_{NI}. All measurements, except those of T_{NI}, were taken at T = 29 °C, f = 1 kHz.

3.3 Particle-laden polymer-stabilized liquid crystal composites

3.3.1 Optical textures. The optical textures of the PLPSLC samples are shown in Fig. 4(a). One can see that small dots started to appear in the textures upon the increase in the particle concentration C_{NP}, and at the highest particle content, a stripe pattern developed. In the image which depicts the cell edge of a PLPSLC sample with C_{NP} = 0.2 wt% (Fig. 4(b-i)), one

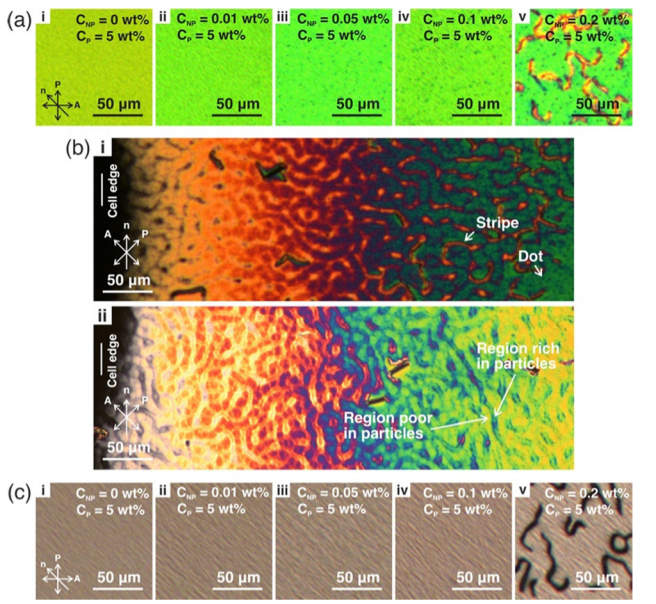

Fig. 4 (a) Polarised optical textures of the PLPSLC composites with different particle concentrations indicated in the images. Images were taken at 29 °C. (b) Polarised optical images of the cell edge for the 5CB + 0.2 wt%PS + 5 wt%RM257 composite after (i) and before (ii) polymerisation. Note that two different areas of the cell are depicted. The images were taken at the room temperature. (c) Polarised optical images of polymer networks formed in the PLPSLC composites with different particle concentrations indicated in the images.

can see that both stripes and dots are part of the pattern running along the edge. The same pattern was observed on the cell periphery in all PLPSLC samples. Notably, the pattern reminds the one observed for the PLLC sample with C_{NP} = 0.2 wt% (Fig. 1(a-vi)). The similarity is more evident from the image of the PLPSLC sample taken before polymerisation (Fig. 4(b-ii)) (which also indicates that the pattern had developed before the network was formed). We propose that the morphological structure in the PLPSLC samples was created through a mechanism similar to the one for the PLLC composites. In this case, it is probable that regions rich and poor in particles are again observed.

In contrast to PLLCs, the worm-like pattern was observed in all PLPSLC samples and was also more pronounced. These two facts may mean that the particle aggregation and sedimentation were enhanced by the presence of the monomers. The possibility of enhancing the aggregation and sedimentation confirms the hypothesis that part of the particles stayed in the bulk in the PLLC systems.

It must be noted that the pattern was much less developed in the distance from the cell edge (compare Fig. 4(a-ii, iii, iv) and (b)). This can be related to the fact that the cell gap decreases when approaching the edge which is confirmed by the colour changing from green to black. The lack of space may promote the particle aggregation (for example, by decreasing the maximum number of particles at the phase interface which the latter can carry) or in some way make the pattern more visible.

The stripes observed at C_{NP} = 0.2 wt% appeared to form in the presumably particle rich regions and resemble linear defects (disclinations) which often form in nematic liquid crystals upon cooling from the isotropic state but usually are unstable and quickly vanish. The stabilisation of such defects by nanodopants has been observed in some of the studies on PLLCs where the sedimentation of functionalized particles and the subsequent creation of the homeotropic alignment have been reported.[49–51] Therefore, the appearance of the defects in the PLPSLC samples indirectly indicates that the particle sedimentation indeed occurred, and the particles most probably kept the surfactant shells. The fact that the defects were observed in only one type of regions supports the suggestion that the discussed areas are rich in particles.

The polarized images of polymer networks formed in the PLPSLC composites are given in Fig. 4(c). As can be seen, the pattern was not templated by the networks. However, certain changes in the network morphology did occur upon the addition of the particles. One can suggest that the polymer strands became less well oriented with increasing C_{NP}, and in the figures, we observe the deviation of the strands from the cell plane. This can be caused by the particle-induced alteration of the surface interactions leading to the distortion of the homogeneous alignment which is then templated by the networks. Since polymer threads are usually about 500 nm in width,[38] the network deformations can additionally be caused by the presence of particle aggregates of a comparable size which act as physical obstacles. A schematic of the resulting network is given in Fig. 5(c-ii) (the particles are not shown).

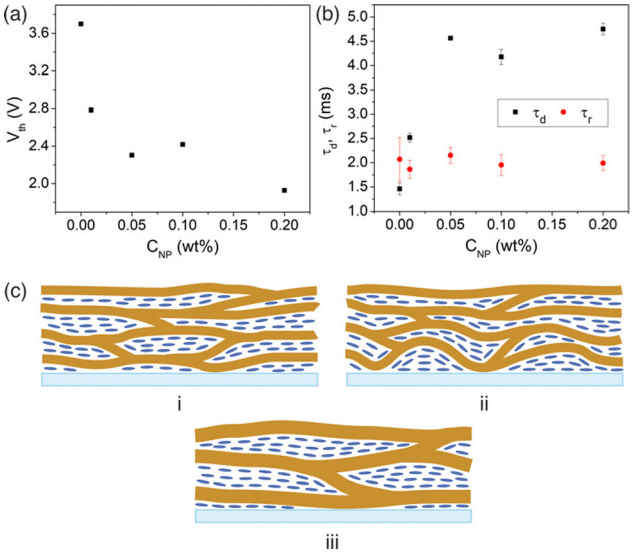

Fig. 5 Dependence of the threshold voltage V_{th} (a) and response times τ_d and τ_r (b) on the particle concentration C_{NP} for the PLPSLC composites. All measurements were taken at T = 29 °C, f = 1 kHz. The rise time τ_r was measured using a carrier signal with a root mean square amplitude of 6 V. (c) (i) Morphology of a polymer network formed in a PSLC system in the vicinity of a cell substrate. (ii and iii) Two hypothetical morphologies of a network formed in a PLPSLC system: a distorted network (ii) and a sparse network with thick polymer strands (iii). The nanoparticles are not shown for the PLPSLC system.

Another possible interpretation of the observed changes in the textures is that the polymer strands became thicker, and, consequently, the network became sparser (Fig. 5(c-iii)). Such effects have been observed in several previous studies on PLPSLCs,[27,30,32] and in study,[32] it has been suggested that the reason behind them is that the particles affect the rate of the polymer–liquid crystal phase separation occurring during polymerisation.[32]

Finally, from Fig. 4(c) also follows that the dots present in the PLPSLC textures (Fig. 4(a-ii)–(a-v)) are not observed in the network images. This fact means that the dots were not large aggregates occupying the whole space between the glass slides but areas where the homogeneous alignment was strongly disturbed. Therefore, they vanished upon the transition to the isotropic state.

3.3.2 Electro-optic properties. According to the graph given in Fig. 5(a), the threshold voltage of the PLPSLC samples showed a noticeable decline with the increase in the particle concentration C_{NP}. The value achieved at the maximum particle concentration C_{NP} = 0.2 wt% was almost twice smaller than that for the PLPSLC sample with C_{NP} = 0 wt%, *i.e.* for the PSLC composite. Such behaviour may be caused by the presumable network distortions caused by the particles. Indeed, the network is well-oriented in the absence of the nanodopants[8,9,38] (Fig. 5(c-i)), and therefore, through the surface interactions, it stabilizes the homogeneous alignment making it more difficult for the liquid crystal molecules to reorient in the direction of the electric field. This results in the threshold voltage increase common for PSLCs. On the other hand, in the presence of the

particles, the homogeneous alignment is distorted: the polymer strands in the vicinity of the substrates do not lie predominantly in the cell plane but deviate from it (Fig. 5(c-ii)) due to the particle-induced director field deformations and the presence of large aggregates. As a result, the tilted parts of the strands promote the tilted orientation of the neighbouring liquid crystal molecules. Since the electric torque acting on such molecules is non-zero, it becomes easier to induce the Freedericks transition. Higher particle concentrations should lead to more significant network distortions, and therefore, V_{th} decreases with increasing C_{NP}.

Another possibility is that the addition of the particles did not lead to a distorted but rather a sparser network with thicker polymer strands[27,30,32] as was discussed in the previous section (Fig. 5(c-iii)). In this case, the total surface area of the polymer–liquid crystal interface should decrease with increasing C_{NP} and in this way weaken the stabilizing effect of the network. This should result in a threshold voltage reduction.

Notably, both discussed interpretations of the threshold voltage decrease mean that the fraction of the network which stabilizes the homogenous alignment reduces when the particle concentration increases. This statement is supported by the way the voltage–capacitance curve $C(V)$ changed with C_{NP}. It can be seen from Fig. 6 that in addition to the lower threshold voltages, the increase in C_{NP} generally resulted in a faster capacitance growth (the larger C_{NP}, the steeper the curve became), and the larger relative change in C being achieved at the maximum voltage. This kind of behaviour is usually observed when the polymer concentration decreases.[37,38] The similarity between the capacitance curve dependence on the polymer and particle content confirms the above statement. For simplicity, one can even say that the effective polymer concentration C_P becomes smaller upon the addition of the particles. Notably, the described changes in $C(V)$ curves have been observed for other PLPSLC systems too.[30,31]

The dependence of the response times on C_{NP} is shown in Fig. 5(b). τ_d first rose and then levelled off at a value which is about 2 times larger than that for the PSLC composite. At the same time, its order of magnitude stayed the same. Since the decay time is known to decline with the polymer concentration,[8,9,39] the observed rise in the property follows from our assumption that the particles decreased the effective C_P. The rise time τ_r was observed to be independent of the particle concentration which may be explained by its weak dependence on C_P in the vicinity of the employed polymer concentration C_P = 5 wt%.

3.3.3 Physical properties. The dielectric constants as a function of particle concentration are shown in Fig. 7(a). Both $\varepsilon_\perp$ and $\varepsilon_\parallel$ increased with increasing C_{NP}. If one assumes that the networks were distorted by the particles (Fig. 5(c-ii)), the increase in the constants can be explained by the presence of the liquid crystal regions influenced by the tilted parts of the polymer strands. Indeed, in the absence of the particles, all molecules affected by the polymer lie mainly in the cell plane and contribute $\varepsilon \approx \varepsilon_\perp^{5CB}$ to $\varepsilon_\perp$ and $\varepsilon_\parallel$ (Fig. 5(c-i)). On the contrary, in the presence of the nanodopants, the network should be distorted, and the molecules affected by the tilted polymer fibres should contribute $\varepsilon > \varepsilon_\perp^{5CB}$ to the overall values of the permittivities increasing the latter. Finally, the dielectric anisotropy showed only a slight decline.

It must be noted that the hypothesis about the sparsening of networks (Fig. 5(c-iii)) also could explain the increase in $\varepsilon_\parallel$ since in this case, more liquid crystal molecules would be allowed to reorient in the electric field due to the decrease in the surface area of the polymer–liquid crystal interface. However, the hypothesis does not predict the observed increase in $\varepsilon_\perp$. Therefore, it is more likely that the addition of the particles resulted in the distortion and not the sparsening of the networks.

Like the threshold voltage, the splay elastic constant K_{11} decreased significantly and became about one order of

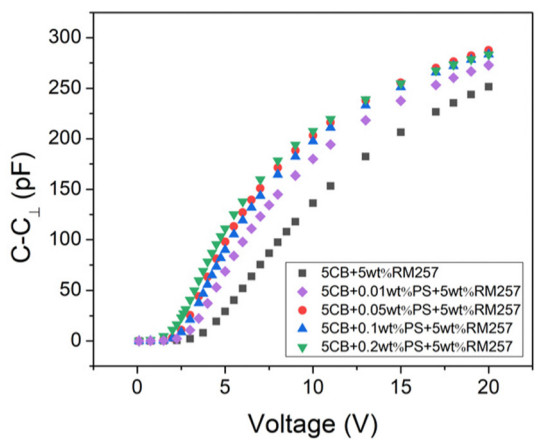

Fig. 6 The dependence of the normalized cell capacitance $C-C_\perp$ on the applied voltage for the PLPSLC composites. All measurements were taken at T = 29 °C, f = 1 kHz.

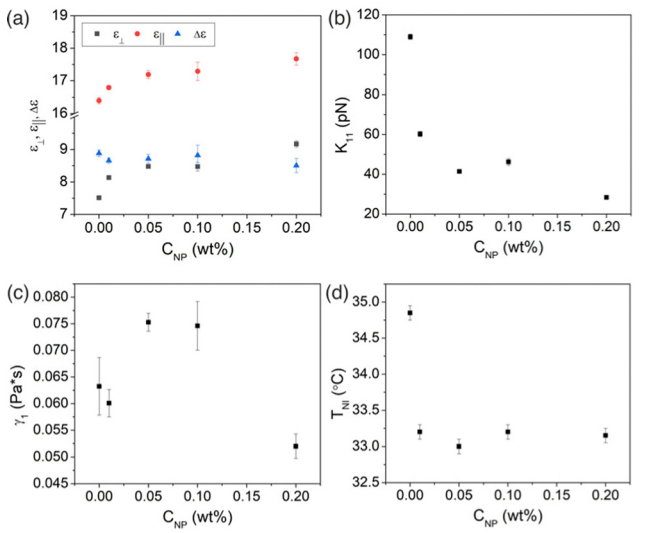

Fig. 7 Dependence of the physical properties on the particle concentration C_{NP} for the PLPSLC composites: (a) the dielectric constants $\varepsilon_\parallel$ and $\varepsilon_\perp$ and dielectric anisotropy $\Delta\varepsilon$, (b) the splay elastic constant K_{11}, (c) the viscosity γ_1, (d) the nematic–isotropic transition temperature T_{NI} (d). All measurements, except those of T_{NI}, were taken at T = 29 °C, f = 1 kHz.

magnitude smaller at the maximum particle concentration C_{NP} = 0.2 wt% (Fig. 7(b)). This agrees with the decrease in the effective polymer concentration since for PSLCs, K_{11} increases with increasing C_P.[9,37]

The viscosity showed a non-monotonic dependence on the particle concentration (Fig. 7(c)). From the lowest concentrations (C_{NP} = 0.01 wt%), it increases, however, later strongly decreases above larger concentrations (C_{NP} = 0.1 wt%). This sudden drop can be related to the formation of stripes (see Fig. 4(a-v)). For example, the main part of particles which did not sediment could accumulate in the defects to stabilize the latter. Therefore, the number of particles left in the generally homogeneous part of the cell decreased. Since the homogeneous part determines most of the optical response, the viscosity measured using the electro-optic curves also decreased.

The phase transition temperature T_{NI} decreased in a stepwise manner (Fig. 7(d)) when simply adding even minute amounts of nanoparticles. The nature of this behaviour has yet to be identified.

3.4 Discussion

Having considered the results for all the three types of composites, let us compare their electro-optic performance. In Fig. 8, the best achieved values of the threshold voltage and response times are given for the PSLC, PLLC, and PLPSLC composites together with values for neat 5CB. As can be seen, polymer stabilisation allowed one to reduce the overall response time of 5CB by about one order of magnitude. However, this improvement was achieved at the cost of the threshold voltage increase by a factor of 6. Such behaviour is common for PSLCs. At the same time, the influence of polystyrene particles on the properties appeared to be relatively weak and mostly negative: V_{th} improved by only 3% while τ_r did not change within the limits of error, and τ_d increased by 21%. Finally, when the particles and the polymer were used together, interesting effects were observed: although the threshold voltage was 3 times as large as the value for pure 5CB, it was reduced by a factor of two in comparison to the PSLC composite. In other words, the problem of high threshold voltages common for polymer-stabilized systems was noticeably alleviated in the case of the PLPSLC composite. Importantly, the response times appeared to be of the same order of magnitude as those for the PSLC sample meaning that the advantage of the fast overall response time provided by the network was retained by the PLPSLC system. To summarize, the PLPSLC composite was optimized only in terms of the overall response time when compared to the liquid crystal. However, its performance was observed to be better than those for both PSLC and PLLC composites individually.

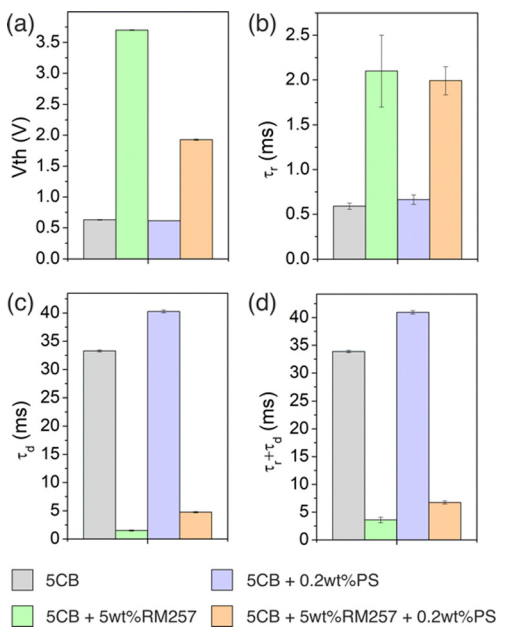

Fig. 8 Comparison of the best achieved values of the electro-optic properties measured for 5CB, PSLC, PLLC, and PLPSLC composites: the best achieved (a) threshold voltages, (b) rise times, (c) decay times, and (d) overall response times.

Let us now compare the results obtained for the polystyrene-PLPSLCs with the previous published work on particle-laden polymer-stabilized liquid crystals. First, the observed threshold voltage reduction in comparison to a polymer-stabilized system with no nanoparticles generally agrees with the behaviour of other PLPSLCs with similar particle concentrations (of less than 3 wt%).[25–27,30,31] The threshold voltage decrease of 50% reported here is relatively large in comparison with a 10–30% reduction observed in studies[25,27,31] and in comparison with studies[27,31] was achieved at a smaller particle concentration (namely, at C_{NP} = 0.2 wt%). However, composites exist which offer better performance. For instance, PLPSLCs doped with only 0.01 wt% of graphene flakes have been shown to reduce V_{th} by a factor of 7 making the latter smaller than even the value for a pure liquid crystal.[30] At the same time, PLPSLCs containing 0.2 wt% of silver nanowires have demonstrated the threshold voltage reduction of 90%.[26] In relation to the response times, the increase in τ_d and no change in τ_r observed in this work contrast with a decrease or no change in these properties reported for other PLPSLCs.[25,27,30,31] However, in both this study and the other articles, the magnitude of the changes does not exceed several tens of percent which is too small to noticably change the speed of a potential device. In general, PLPSLCs doped with polystyrene nanoparticles demonstrated relatively good performance in comparison with the other systems of the same type.

In the end, it must be highlighted that to explain the obtained results, we suggested that the polystyrene particles decreased the effective polymer concentration. This fact raises a question whether such particles can be of practical use if one can directly change the polymer content to achieve the same result. Further research is necessary to reliably confirm the suggested explanation model and answer this question.

4. Conclusions

In this work, the electro-optic properties of polystyrene particle-laden polymer-stabilized liquid crystal composites were

studied. First, we characterized PSLC and PLLC systems made of target materials. For the PSLC composite, the overall response time was decreased compared to 5CB but at the cost of the increased threshold voltage. At the same time, the electro-optic properties of PLLCs differed from those of the liquid crystal relatively slightly. Importantly, combining the particles and the polymer helped to achieve a performance which is better compared to both PLLC and PSLC systems: the PLPSLC composites turned out to be almost as fast as the PSLC system, *i.e.* much faster than the liquid crystal, but, at the same time, could be operated by lower voltages.

The observed effects were assigned to the decrease in the effective polymer concentration presumably caused by either the particle-induced distortion or particle-induced sparsening of the polymer network. This fact questions the necessity of adding polystyrene particles since the polymer content can be directly tuned instead. However, further research is still necessary to reliably confirm the suggested explanation model. Nevertheless, we hope that the reported results will help to shed light on how simple nanoparticles without distinctive physical properties interact with the polymer network and liquid crystal since this knowledge can potentially aid the creation of more complex PLPSLC composites in the future.

Author contributions

The work presented here was conceived and supervised by ID. AG carried out the experimental measurements and the data analysis. All authors contributed to the writing of the manuscript.

Conflicts of interest

The authors declare no conflicts of interest.

References

1 R. H. Chen, *Liquid Crystal Displays: Fundamental Physics and Technology*, John Wiley & Sons, Inc., 2011.
2 G. F. Sung, P. C. Wu, V. Y. Zyryanov and W. Lee, Electrically active and thermally passive liquid-crystal device toward smart glass, *Photon Res, PRJ.*, 2021, **9**(11), 2288–2295, DOI: **10.1364/PRJ.437654**.
3 W. F. Chiang, H. M. Silalahi and Y. C. Chiang, *et al.*, Continuously tunable intensity modulators with large switching contrasts using liquid crystal elastomer films that are deposited with terahertz metamaterials, *Opt Express*, 2020, **28**(19), 27676–27687, DOI: **10.1364/OE.399581**.
4 C. R. Lee, S. H. Lin and S. M. Wang, *et al.*, Optically controllable photonic crystals and passively tunable terahertz metamaterials using dye-doped liquid crystal cells, *J Mater Chem C*, 2018, **6**(18), 4959–4966, DOI: **10.1039/C7TC05724E**.
5 Y. Xie, T. Lei and D. Wang, *et al.*, High-speed Stokes vector receiver enabled by a spin-dependent optical grating, *Photonics Res.*, 2021, **9**(8), 1470–1476, DOI: **10.1364/PRJ.416376**.
6 H. Coles and S. Morris, Liquid-crystal lasers, *Nat. Photon*, 2010, **4**(10), 676–685, DOI: **10.1038/nphoton.2010.184**.
7 I. Dierking, *Polymer-Modified Liquid Crystals*, The Royal Society of Chemistry, 2019.
8 P. A. Kossyrev, J. Qi, N. V. Priezjev, R. A. Pelcovits and G. P. Crawford, Virtual surfaces, director domains, and the Fréedericksz transition in polymer-stabilized nematic liquid crystals, *Appl. Phys. Lett.*, 2002, **81**(16), 2986–2988, DOI: **10.1063/1.1515136**.
9 P. L. Madhuri, U. S. Hiremath, C. V. Yelamaggad, K. P. Madhuri and S. K. Prasad, Influence of virtual surfaces on Frank elastic constants in a polymer-stabilized bent-core nematic liquid crystal, *Phys Rev E*, 2016, **93**(4), 042706, DOI: **10.1103/PhysRevE.93.042706**.
10 C. Y. Huang, W. Y. Jhuang and C. T. Hsieh, Switching of polymer-stabilized vertical alignment liquid crystal cell, *Opt Express*, 2008, **16**(6), 3859–3864, DOI: **10.1364/OE.16.003859**.
11 M. J. Escuti, C. C. Bowley, G. P. Crawford and S. Žumer, Enhanced dynamic response of the in-plane switching liquid crystal display mode through polymer stabilization, *Appl. Phys. Lett.*, 1999, **75**(21), 3264–3266, DOI: **10.1063/1.125319**.
12 Y. Q. Lu, F. Du, Y. H. Lin and S. T. Wu, Variable optical attenuator based on polymer stabilized twisted nematic liquid crystal, *Opt Express*, 2004, **12**(7), 1221–1227, DOI: **10.1364/OPEX.12.001221**.
13 Y. Reznikov, O. Buchnev, O. Tereshchenko, V. Reshetnyak, A. Glushchenko and J. West, Ferroelectric nematic suspension, *Appl. Phys. Lett.*, 2003, **82**(12), 1917–1919, DOI: **10.1063/1.1560871**.
14 H. H. M. Elkhalgi, S. Khandka, U. B. Singh, K. L. Pandey, R. Dabrowski and R. Dhar, Dielectric and electro-optical properties of a nematic liquid crystalline material with gold nanoparticles, *Liq. Cryst.*, 2018, **45**(12), 1795–1801, DOI: **10.1080/02678292.2018.1487089**.
15 C. W. Oh, E. G. Park and H. G. Park, Enhanced electro-optical properties in titanium silicon oxide nanoparticle doped nematic liquid crystal system, *Surf. Coat. Technol.*, 2019, **360**, 50–55, DOI: **10.1016/j.surfcoat.2019.01.014**.
16 B. Kinkead and T. Hegmann, Effects of size, capping agent, and concentration of CdSe and CdTe quantum dots doped into a nematic liquid crystal on the optical and electro-optic properties of the final colloidal liquid crystal mixture, *J. Mater. Chem.*, 2009, **20**(3), 448–458, DOI: **10.1039/B911641A**.
17 S. E. San, M. Okutan, O. Köysal and Y. Yerli, Carbon Nanoparticles in Nematic Liquid Crystals, *Chin. Phys Lett.*, 2008, **25**(1), 212, DOI: **10.1088/0256-307X/25/1/058**.
18 I. S. Baik, S. Y. Jeon and S. H. Lee, *et al.*, Electrical-field effect on carbon nanotubes in a twisted nematic liquid crystal cell, *Appl. Phys. Lett.*, 2005, **87**(26), 263110, DOI: **10.1063/1.2158509**.

19 Ş. Özgan, H. Eskalen and Y. Tapkıranlı, Thermal and electro-optic properties of graphene oxide-doped hexylcyanobiphenyl liquid crystal, *J Theor Appl Phys.*, 2018, **12**(3), 169–176, DOI: 10.1007/s40094-018-0307-y.

20 S. Y. Lu and L. C. Chien, Carbon nanotube doped liquid crystal OCB cells: physical and electro-optical properties, *Opt Express*, 2008, **16**(17), 12777–12785, DOI: 10.1364/OE.16.012777.

21 M. E. Abbasov and G. O. Carlisle, Effects of carbon nanotubes on electro-optical properties of dye-doped nematic liquid crystal, *J. Mater. Sci.: Mater. Electron.*, 2012, **23**(3), 712–717, DOI: 10.1007/s10854-011-0477-8.

22 R. Basu and G. S. Iannacchione, Dielectric hysteresis, relaxation dynamics, and nonvolatile memory effect in carbon nanotube dispersed liquid crystal, *J. Appl. Phys.*, 2009, **106**(12), 124312, DOI: 10.1063/1.3272080.

23 A. Glushchenko, C. I. Cheon and J. West, *et al.*, Ferroelectric Particles in Liquid Crystals: Recent Frontiers, *Mol. Cryst. Liq. Cryst.*, 2006, **453**(1), 227–237, DOI: 10.1080/15421400600653852.

24 S. Klein, R. M. Richardson and R. Greasty, *et al.*, The influence of suspended nanoparticles on the Frederiks threshold of the nematic host, *Philos. Trans. R. Soc., A*, 2013, **371**(1988), 20120253, DOI: 10.1098/rsta.2012.0253.

25 X. Yan, Y. Zhou and W. Liu, *et al.*, Effects of silver nanoparticle doping on the electro-optical properties of polymer stabilized liquid crystal devices, *Liq. Cryst.*, 2020, **47**(8), 1131–1138, DOI: 10.1080/02678292.2019.1641754.

26 X. Yan, W. Liu and Y. Zhou, *et al.*, Improvement of Electro-Optical Properties of PSLC Devices by Silver Nanowire Doping, *Appl. Sci.*, 2019, **9**(1), 145, DOI: 10.3390/app9010145.

27 G. Kocakülah, G. Algül and O. Köysal, Effect of CdSeS/ZnS quantum dot concentration on the electro-optical and dielectric properties of polymer stabilized liquid crystal, *J. Mol. Liq.*, 2020, **299**, 112182, DOI: 10.1016/j.molliq.2019.112182.

28 O. V. Yaroshchuk, L. O. Dolgov and A. D. Kiselev, Electro-optics and structural peculiarities of liquid crystal–nanoparticle-polymer composites, *Phys Rev E*, 2005, **72**(5), 051715, DOI: 10.1103/PhysRevE.72.051715.

29 L. Dolgov and O. Yaroshchuk, Electro-optics of Suspensions of Monodispersed Inorganic Nanoparticles in Liquid Crystals, *Mol. Cryst. Liq. Cryst.*, 2004, **409**(1), 77–89, DOI: 10.1080/15421400490435783.

30 M. Baral, K. Bramhaiah, N. S. John and S. Krishna Prasad, Graphene-Augmented Polymer Stabilization: Drastically Reduced and Temperature-Independent Threshold and Improved Contrast Liquid Crystal Device, *ACS Omega*, 2019, **4**(1), 403–411, DOI: 10.1021/acsomega.8b03026.

31 S. Krishna Prasad, M. Baral, A. Murali and S. N. Jaisankar, Carbon Nanotube Reinforced Polymer-Stabilized Liquid Crystal Device: Lowered and Thermally Invariant Threshold with Accelerated Dynamics, *ACS Appl. Mater. Interfaces*, 2017, **9**(31), 26622–26629, DOI: 10.1021/acsami.7b08825.

32 Z. Zhang, R. Zhang and L. Xu, *et al.*, Visible and infrared optical modulation of PSLC smart films doped with ATO nanoparticles, *Dalton Trans.*, 2021, **50**(29), 10033–10040, DOI: 10.1039/D1DT01575C.

33 C. J. Hsu, C. C. Kuo, C. D. Hsieh and C. Y. Huang, Effects of silica nanoparticles on electro-optical properties of polymer-stabilized liquid crystals, *Opt Express*, 2014, **22**(15), 18513–18518, DOI: 10.1364/OE.22.018513.

34 T. Uchida and Y. Takahashi, New Method to Determine Elastic Constants of Nematic Liquid Crystal From C-V Curve, *Mol. Cryst. Liq. Cryst.*, 1981, **72**(4), 133–137, DOI: 10.1080/01406568108084049.

35 L. M. Blinov, *Structure and Properties of Liquid Crystals*, Springer Dordrecht, 2011.

36 L. M. Blinov and V. G. Chigrinov, *Electrooptic Effects in Liquid Crystal Materials*, Springer, 1996.

37 N. Dessaud, P. Raynes and P. Bonnett, Dielectric behavior of polymer-stabilized-liquid-crystal cells made from hosts with different ultraviolet absorptions, *J. Appl. Phys.*, 2004, **96**(8), 4366–4371, DOI: 10.1063/1.1790589.

38 R. Q. Ma and D. K. Yang, Freedericksz transition in polymer-stabilized nematic liquid crystals, *Phys Rev E*, 2000, **61**(2), 1567–1573, DOI: 10.1103/PhysRevE.61.1567.

39 S. Mora, A. M. Jamieson and L. C. Chien, Freedericksz Transition Measurements on Polymer-Stabilized Liquid Crystals, *Mol. Cryst. Liq. Cryst. Sci. Technol., Sect. A*, 1997, **292**(1), 323–331, DOI: 10.1080/10587259708031941.

40 M. Pande, P. K. Tripathi, A. K. Misra, S. Manohar, R. Manohar and S. Singh, Dielectric and electro-optical properties of polymer-stabilized liquid crystal system, *Appl. Phys. A: Mater. Sci. Process.*, 2016, **122**(3), 217, DOI: 10.1007/s00339-016-9749-8.

41 P. Satapathy, S. Parthasarathi, D. S. S. Rao, S. Bano, Y. S. Negi and S. K. Prasad, Switchable smart windows using a biopolymer network of cellulose nanocrystals imposed on a nematic liquid crystal, *Appl. Phys. Lett.*, 2020, **117**(10), 103702, DOI: 10.1063/5.0020982.

42 A. Matsuyama, Morphology of spinodal decompositions in liquid crystal–colloid mixtures, *J. Chem. Phys.*, 2008, **128**(22), 224907, DOI: 10.1063/1.2936831.

43 P. Dayal, R. A. Matkar and T. Kyu, Crystal-liquid crystal binary phase diagrams, *J. Chem. Phys.*, 2006, **124**(22), 224902, DOI: 10.1063/1.2200688.

44 A. Matsuyama and R. Hirashima, Phase separations in liquid crystal-colloid mixtures, *J. Chem. Phys.*, 2008, **128**(4), 044907, DOI: 10.1063/1.2823737.

45 A. Matsuyama, Phase separations in mixtures of a liquid crystal and a nanocolloidal particle, *J. Chem. Phys.*, 2009, **131**(20), 204904, DOI: 10.1063/1.3266509.

46 J. Mirzaei, M. Urbanski, H. S. Kitzerow and T. Hegmann, Hydrophobic gold nanoparticles via silane conjugation: chemically and thermally robust nanoparticles as dopants for nematic liquid crystals, *Philos. Trans. R. Soc., A*, 2013, **371**(1988), 20120256, DOI: 10.1098/rsta.2012.0256.

47 H. Qi and T. Hegmann, Multiple Alignment Modes for Nematic Liquid Crystals Doped with Alkylthiol-Capped Gold Nanoparticles, *ACS Appl. Mater. Interfaces*, 2009, **1**(8), 1731–1738, DOI: 10.1021/am9002815.

48 M. Urbanski, J. Mirzaei, T. Hegmann and H. S. Kitzerow, Nanoparticle Doping in Nematic Liquid Crystals: Distinction between Surface and Bulk Effects by Numerical Simulations, *Chem. Phys. Chem.*, 2014, **15**(7), 1395–1404, DOI: **10.1002/cphc.201301054**.

49 H. Qi, B. Kinkead and T. Hegmann, Unprecedented Dual Alignment Mode and Freedericksz Transition in Planar Nematic Liquid Crystal Cells Doped with Gold Nanoclusters, *Adv. Funct. Mater.*, 2008, **18**(2), 212–221, DOI: **10.1002/adfm.200701327**.

50 B. Kinkead, M. Urbanski, H. Qi, H. S. Kitzerow and T. Hegmann, Alignment and electrooptic effects in nanoparticle-doped nematic liquid crystals, in *Liquid Crystals XIV*, SPIE, 2010, vol. 7775, 60–70. , DOI: **10.1117/12.858831**.

51 H. Qi and T. Hegmann, Formation of periodic stripe patterns in nematic liquid crystals doped with functionalized gold nanoparticles, *J. Mater. Chem.*, 2006, **16**(43), 4197–4205, DOI: **10.1039/B611501B**.

52 M. Urbanski, On the impact of nanoparticle doping on the electro-optic response of nematic hosts, *Liquid Crystals Today*, 2015, **24**(4), 102–115, DOI: **10.1080/1358314X.2015.1059586**.

53 P. K. C. Pillai and Rashmi, Dielectric Properties of Polystyrene and Some Related Polymers, *Int. J. Polym. Mater. Polym. Biomater.*, 1980, **8**(4), 255–263, DOI: **10.1080/00914038008077953**.

54 K. K. Vardanyan, D. M. Sita, R. D. Walton, W. M. Saidel and K. M. Jones, Cyanobiphenyl liquid crystal composites with gold nanoparticles, *RSC Adv.*, 2012, **3**(1), 259–273, DOI: **10.1039/C2RA21220J**.

55 K. K. Vardanyan, E. D. Palazzo and R. D. Walton, Nematic nanocomposites with enhanced optical birefringence, *Liq. Cryst.*, 2011, **38**(6), 709–715, DOI: **10.1080/02678292.2011.569760**.

56 H. Ayeb, S. Alaya and M. Derbali, *et al.*, Dielectrical, electro-optical and textural studies of 5CB nematic liquid crystal doped with TiO2 and Cu-TiO2 nanoparticle, *Liq. Cryst.*, 2021, **48**(2), 223–232, DOI: **10.1080/02678292.2020.1771784**.

57 D. N. Chausov, A. D. Kurilov, R. N. Kucherov, A. V. Simakin and S. V. Gudkov, Electro-optical performance of nematic liquid crystals doped with gold nanoparticles, *J. Phys: Condens Matter.*, 2020, **32**(39), 395102, DOI: **10.1088/1361-648X/ab966c**.

58 E. B. Barmatov, D. A. Pebalk and M. V. Barmatova, Influence of silver nanoparticles on the order parameter of liquid crystalline polymers, *Liq. Cryst.*, 2006, **33**(9), 1059–1063, DOI: **10.1080/02678290600898484**.

59 G. Sinha, C. Glorieux and J. Thoen, Broadband dielectric spectroscopy study of molecular dynamics in the glass-forming liquid crystal isopentylcyanobiphenyl dispersed with aerosils, *Phys Rev E*, 2004, **69**(3), 031707, DOI: **10.1103/PhysRevE.69.031707**.

60 P. Kopčanský, N. Tomašovičová and M. Koneracká, *et al.*, Structural Phase Transition in Liquid Crystal Doped with Gold Nanoparticles, *Acta Phys. Pol., A*, 2010, **118**(5), 988–989, DOI: **10.12693/APhysPolA.118.988**.

61 M. V. Gorkunov and M. A. Osipov, Mean-field theory of a nematic liquid crystal doped with anisotropic nanoparticles, *Soft Matter*, 2011, **7**(9), 4348–4356, DOI: **10.1039/C0SM01398F**.